ACS OMEGA

http://pubs.acs.org/journal/acsodf

Article

Shape Matters: The Effect of Particle Morphology on the Fast-Charging Performance of $LiFePO_4$/C Nanoparticle Composite Electrodes

Julia Seher and Michael Fröba*

Cite This: https://doi.org/10.1021/acsomega.1c03432

Read Online

ACCESS | Metrics & More | Article Recommendations | Supporting Information

ABSTRACT: For the successful use of lithium-ion batteries in automotive applications, reliable availability of high storage capacity and very short recharging times are essential. In order to develop the perfect battery for a certain application, structure−property relationships of each active material must be fully understood. $LiFePO_4$ is of great interest due to its fast-charging capability and high stability regarding its thermal resistance and chemical reactivity. The anisotropic lithium-ion diffusion through the $LiFePO_4$ crystal structure indicates a strong dependence of the electrochemical performance of a nanostructured active material on particle morphology. In this paper, the relationship of the particle morphology and fast-charging capability of $LiFePO_4$/C core/shell nanoparticles in half-cells was studied. For this purpose, a new multistep synthesis strategy was developed. It involves the combination of a solvothermal synthesis followed by an *in situ* polymer coating and thermal calcination step. Monodisperse rodlike $LiFePO_4$ nanoparticles with comparable elongation along the *b*-axis (30−50 nm) and a varying aspect ratio *c*/*a* (2.4−6.9) were obtained. A strong correlation of the fast-charging capability with the aspect ratio *c*/*a* was observed. When using $LiFePO_4$ nanoparticles with the smallest aspect ratio *c*/*a*, the best electrochemical performance was received regarding the specific capacity at high C-rates and the cycling stability. A reduction of the aspect ratio *c*/*a* by 30% (3.6 to 2.4) was found to enhance the charge capacity at 10 C up to an order of magnitude (7.4−73 mA h·g^{-1}).

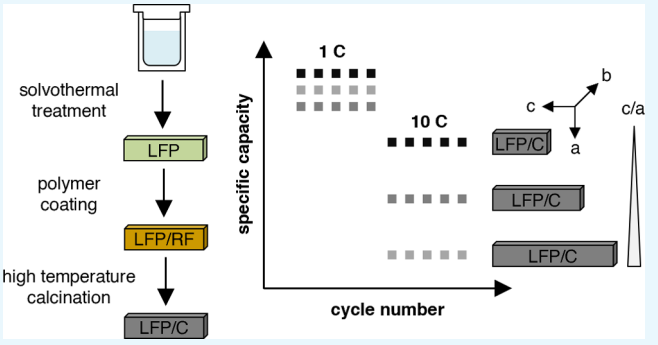

INTRODUCTION

The commercial launch of lithium-ion batteries in 1991 and their subsequent development were the key factors enabling the rise and global distribution of portable communications and consumer electronics that we see today. However, another pivotal role for lithium-ion batteries will be enabling zero-emission mobility by powering electric vehicles. Batteries with high energy storage capacity and fast-charging capability are needed to make electric vehicles competitive to vehicles with an internal combustion engine with no disadvantages or restrictions for drivers. In order to develop new battery cells, structure−property relationships must be fully understood to unlock the full potential of active materials by specific modification strategies.

$LiFePO_4$ is already being used commercially as a cathode material in secondary lithium-ion batteries. Due to its high thermal and chemical stability and its fast-charging capability, it is of great interest for the application in electric vehicles.[1] Due to its low ionic and electric conductivity, $LiFePO_4$ in its bulk form was initially classified as unsuitable for fast-charging applications.[2] Over the last 20 years, countless synthetic methods were reported to enhance the electrochemical properties of $LiFePO_4$-based electrodes.[3,4] The most important strategies are the reduction of the diffusion paths by nanostructuring, the modification of the crystal structure by doping, and the modification of the crystal surface by a coating with a more conductive material such as carbon.[5−10]

Carbon coating can be carried out *ex situ* or *in situ*. Basically, any organic compound with a high degree of sp^2-hybridized carbon atoms can be considered, as long as it can be transformed to a carbon shell with a suitable degree of graphitization. For solution-based syntheses, of course, the solubility of the carbon precursor is crucial. Even $LiFePO_4$/C composites consisting of graphene were studied and show impressive electrochemical performance at high C-rates.[11−15] The optimal carbon content and shell thickness of $LiFePO_4$/C composite materials depend on the specific composite structure with the quality of the carbon coating being the most important aspect. $LiFePO_4$ particles have to be covered

Received: June 30, 2021
Accepted: August 4, 2021

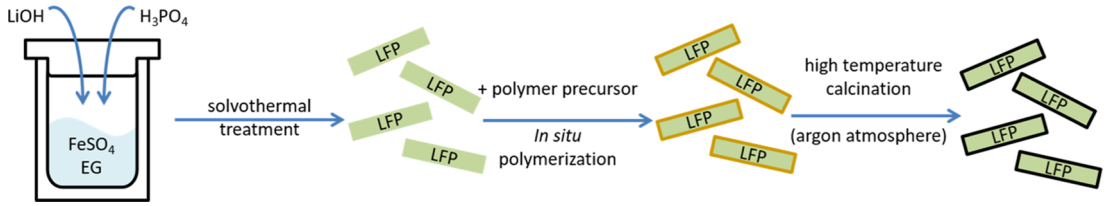

Figure 1. Schematic illustration of the three-step synthesis pathway.

with a homogeneous carbon layer, exhibiting a continuous carbon network. Based on literature reports, the carbon content should not be greater than 10 wt % and the shell thickness should not be below 10 nm to achieve optimal results.[6,7,16]

Despite the anisotropic lithium-ion diffusion in $LiFePO_4$ that takes place exclusively along the crystallographic *b*-axis and the two-phase transition involved in the transformation from $LiFePO_4$ to $FePO_4$, nanostructured $LiFePO_4$/C materials exhibit fast-charging capabilities. Utilizing modern *in situ* characterization methods, it could be shown that at high C-rates, the phase transformation takes place via a metastable transition state and without phase separation, which explains the unique fast-charging and discharging capability of $LiFePO_4$.[17−19] Both theoretical and experimental literature reports indicate that a short elongation along the *b* axis, as well as a large share of (010) facets, enhances the electrochemical performance of $LiFePO_4$/C composite materials. Different studies compared $LiFePO_4$ nanoparticles regarding their morphology. Mostly, plate- and rodlike nanoparticles showed the best electrochemical performance almost up to the maximum of theoretical capacity.[2029] In general, however, the material with the shortest dimension along the *b*-axis showed the best electrochemical performance independent of its morphology. Despite the numerous studies, the influence of the morphology alone on capacity and the fast-charging performance is not fully understood.

To improve the understanding of the influence of the elongation along crystallographic axes other than the *b* axis on their electrochemical properties, we studied carbon-coated $LiFePO_4$ nanoparticles with identical dimension along the *b* axis but different aspect ratios *c*/*a*. $LiFePO_4$/C core/shell particles were obtained through a new multistep synthetic route. To produce a homogeneous carbon shell around each individual $LiFePO_4$ particle, a polymer coating based on resorcinol−formaldehyde was performed. By calcination, the polymer coating was transformed to an amorphous, non-graphitic carbon shell. The main focus of the material characterization was on the electrochemical performance, especially on the fast-charging capability of the $LiFePO_4$ materials as a function of the individual nanoparticles' aspect ratio *c*/*a*.

While the variation of the carbon source can also strongly affect the absolute capacity values, this aspect was not investigated further in this paper as its focus was to study the influence of the morphology variation alone on electrochemical properties. Another issue is addressed in this paper: the exact differentiation between charge and discharge capacity and a detailed listing of the measurement parameters of the electrochemical characterization are rarely carried out, which limits the comparability of published results on the fast-charging capability of $LiFePO_4$ materials. Although the discharge capacity represents the energy that a consumer can actually use from a charged battery, the obtained values for the specific capacity at fast-discharging are not identical to the one under fast-charging conditions, especially if the battery cell was previously charged at a low C-rate. Therefore, our fast-charging and -discharging tests were carried out under standardized and comparable conditions. For this purpose, a commercial test cell with a fixed cell design was used which reduces the individual influence of the user during cell assembly to a minimum.

RESULTS AND DISCUSSION

A multistep synthesis was developed based on a new combination of the known synthesis strategies[25,30−33] to produce $LiFePO_4$/C core/shell nanoparticles with a homogeneous carbon shell and different $LiFePO_4$ particle sizes and morphologies. The synthesis pathway can be divided into three steps: (1) solvothermal synthesis of $LiFePO_4$ nanoparticles, (2) synthesis of $LiFePO_4$/RF core/shell particles via polymer coating with *in situ*-formed resorcinol−formaldehyde resin, and (3) synthesis of $LiFePO_4$/C core/shell nanoparticles via calcination of $LiFePO_4$/RF core/shell particles in an inert atmosphere (Figure 1). The synthesis of $LiFePO_4$ via a solvothermal synthesis in ethylene glycol provides monodisperse $LiFePO_4$ nanoparticles with a specific morphology. Ethylene glycol acts as a solvent, surfactant, and reducing agent at the same time. The adsorption of ethylene glycol takes place preferentially at the (010) plane, which inhibits the particle growth parallel to [010], which results in plate-like and rodlike $LiFePO_4$ nanoparticles.[27,34] Particle size and particle morphology remain unchanged during polymer coating and calcination. Although additional synthesis steps are required, carbon coating via an intermediate polymer coating step provides homogenous carbon shells, which is difficult to obtain with conventional coating methods using a sugar or other carbon-rich components via one-step syntheses.[35]

A set of five materials composed of rod-shaped $LiFePO_4$/C core/shell nanoparticles, which differ in elongation and aspect ratio, was synthesized to study the influence of morphology on the fast-charging performance. The elongation of the $LiFePO_4$ rod-shaped particles was tuned by the Li/Fe/P ratio and the pH value in the starting solution. All materials consist of pristine olivine-type $LiFePO_4$ based on the X-ray diffraction data without additional peaks (Figure 2). In addition, no evidence of the carbon shells was provided by X-ray diffraction, which indicates that the shell thickness is extremely thin and amorphous.

In preliminary tests, a carbon content of 9.5 wt % and a carbon shell thickness d_s of 7 nm were found as optimum regarding fast-charging performance. In the case of the five $LiFePO_4$/C materials, the carbon content average was 9.7 wt %, which was determined with CHNS analysis. Individual values for each material are summarized in Table 1. The carbon shell thickness and the particle size were determined using electron microscopy. Transmission electron microscopy

https://doi.org/10.1021/acsomega.1c03432
ACS Omega XXXX, XXX, XXX−XXX

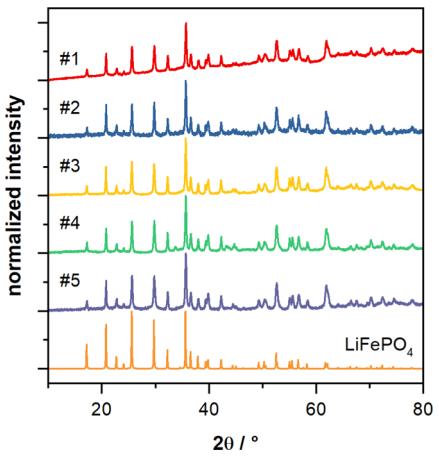

Figure 2. X-ray diffraction patterns of all $LiFePO_4$/C core/shell nanoparticles and the reference pattern of $LiFePO_4$ (COD 2100916).

Table 1. Summary of Structural Values of all $LiFePO_4$/C Core/shell Nanoparticle Materials

#	c (nm)	a (nm)	c/a	d_S (nm)	m_C (wt %)
1	310	45	6.9	6	8.6
2	290	80	3.6	7	9.5
3	190	60	3.2	5	11.9
4	165	70	2.4	5	9.4
5	135	55	2.5	2	9.1

(TEM) images of all materials are presented in Figure 3. Their rod-shaped morphology and the core/shell structure could be confirmed. The average carbon shell thickness was 5 nm.

Nitrogen physisorption measurement yielded type I physisorption isotherms with a type H4 hysteresis loop for all materials. Assuming a compact $LiFePO_4$ core, this indicates that the carbon shells consist of microporous aggregates as the nitrogen can only adsorb on the carbon surface (Figure S1).

The crystal orientation was identified using a software-supported analysis[36] of the electron diffraction patterns. For each material, [010] was determined as the zone axis (Figure 4). The largest elongation is along c, and the shortest elongation is along b. The main exposed plane is (010), while the elongation along b is for all materials in the same range (30−50 nm). The aspect ratio of the particle elongation parallel to the crystallographic axes c and a (c/a) is between 2.4 and 6.9.

To evaluate the electrochemical performance of the five $LiFePO_4$/C composite materials, several electrochemical tests were performed. In the first step, a stability test at 1 C was carried out. Half cells of each material were cycled 500 times. Figure 5 shows the obtained results. After an initial capacity loss during the first cycles, all materials show a very stable behavior over 500 cycles. A slight oscillation of the measured capacity values is observed, which is caused by small day and night variations at room temperature during measurements. The specific charging capacities after 500 cycles are between 77.4 and 84.9 mA $h \cdot g^{-1}$. Only the material with c/a = 3.2 shows a lower charging capacity. This could be due to its slightly higher carbon content (11.9 wt %) and therefore lower amount of $LiFePO_4$ and mobile lithium ions per gram cathode material. In this work, C-rates and specific capacities were defined in relation to the total mass of the cathode material ($LiFePO_4$ + carbon shell); therefore, a decrease in specific capacity by decreasing the amount of $LiFePO_4$ content is reasonable.

After determining long-term electrochemical stability of the materials, their fast-charging behavior was tested. For this purpose, test cells were charged and discharged at C-rates from 0.05 to 10 C. Charge and discharge rates were identical. To study the cycle stability at different C-rates, the test was repeated three times. All results are shown in Figure 6. In general, all materials show stable behavior. Up to 5 C, all materials could be charged and discharged, while the specific capacity decreased with increasing C-rate. A dependency of the achieved specific capacities on the composition of the $LiFePO_4$/C composite materials could be found for C-rates up to 2 C. The material with c/a = 3.2 and with the highest carbon content and the lowest $LiFePO_4$ content exhibits the

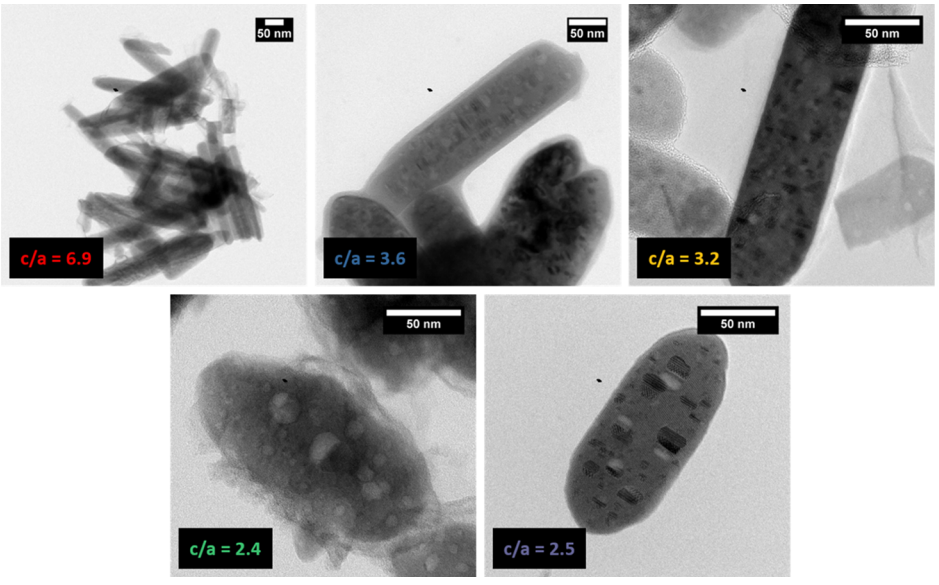

Figure 3. TEM images of rod-shaped $LiFePO_4$/C core/shell nanoparticles with different aspect ratios regarding their dimension along crystallographic axes c and a.

https://doi.org/10.1021/acsomega.1c03432
ACS Omega XXXX, XXX, XXX−XXX

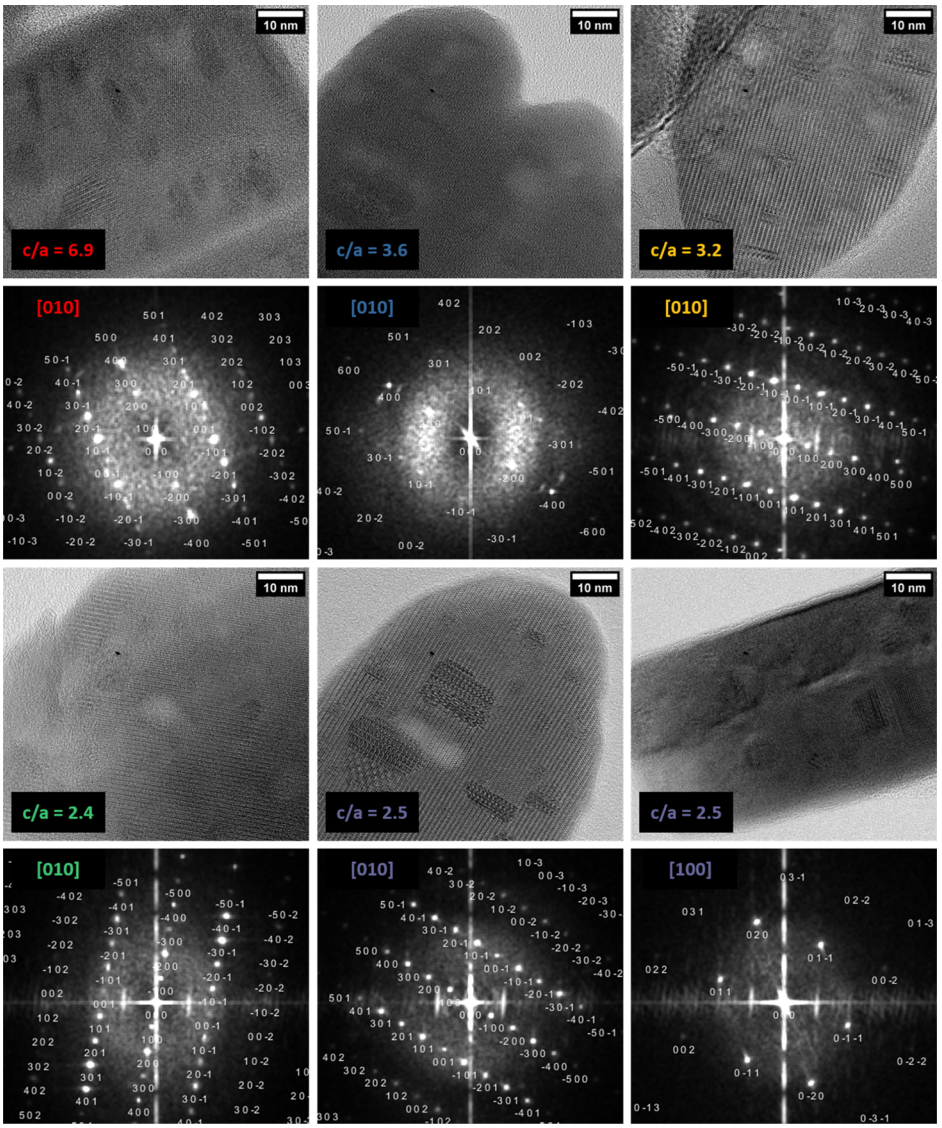

Figure 4. Identification of LiFePO4 nanocrystal orientation by software-supported analysis of electron diffraction patterns.

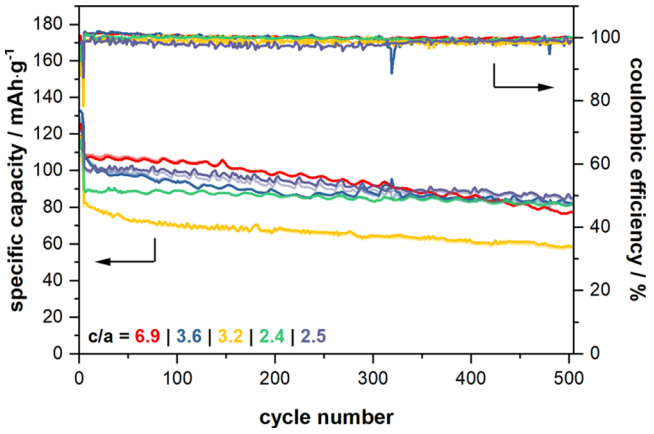

Figure 5. Electrochemical stability test: test cells were cycled 500 times at 1 C.

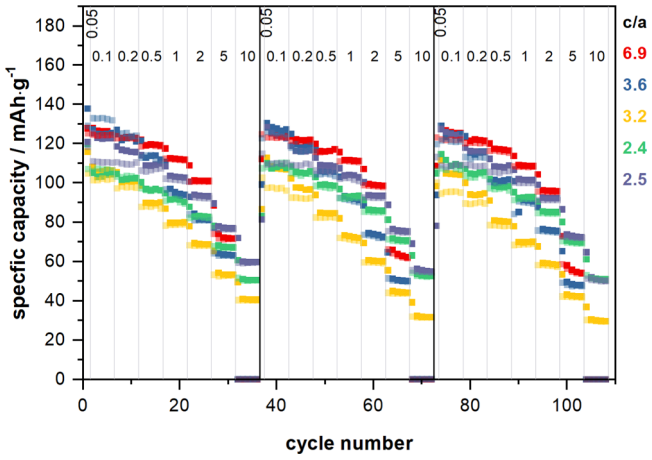

Figure 6. Fast-charging test I: cells were charged at different C-rates (0.05−10 C CC) and discharged with the same C-rate as charged.

lowest specific capacity, while the material with c/a = 6.9 and with the lowest carbon content and the highest $LiFePO_4$ content shows the highest specific capacity. The obtained results show that the lithium diffusion during charge and discharge at C-rates up to 2 C can take place unhindered, so that the available specific capacity depends only on the amount of charge carriers or lithium ions, respectively.

https://doi.org/10.1021/acsomega.1c03432
ACS Omega XXXX, XXX, XXX−XXX

At 10 C, only the materials with a low aspect ratio (2.4−3.2) could be reversibly charged and discharged. The material with the lowest aspect ratio obtained the highest values for specific charge and discharge capacity. In conclusion, at high C-rates, the aspect ratio c/a or the rod-shaped $LiFePO_4$/C core/shell particles influenced the electrochemical performance. This finding is in agreement with results by Muraliganth et al. who studied the discharge behavior at 10 C of two composite materials consisting of rod-shaped $LiFePO_4$ and multiwalled carbon nanotubes with different aspect ratios.[20]

The dependency of the electrochemical performance on the aspect ratio c/a and the length of the rod-shaped $LiFePO_4$ nanoparticles could be confirmed with a second fast-charging test. The test cells were charged at C-rates from 0.5 to 10 C and discharged always at 0.5 C. Charging at various C-rates and discharging at a constant lower C-rate are more realistic in terms of the application of lithium-ion batteries. Consumers wish to charge mobile phones or battery electric vehicle in the shortest possible time and use the electronic device for a long period of time. Figure 7 shows the results of the second fast-charging test.

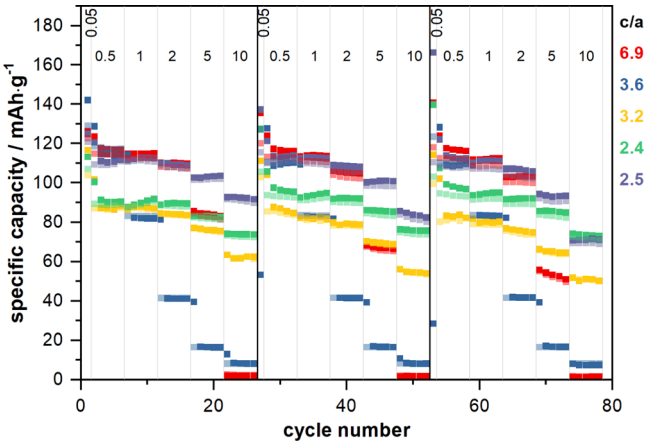

Figure 7. Fast-charging test II: cells were charged at different C-rates (0.05−10 C CC) and discharged at 0.5 C CC.

All cells were very stable. The absolute values of specific capacity are up to 10 mA $h \cdot g^{-1}$ greater than in the first fast-charging test. With a small discharge rate of 0.5 C, a complete lithiation to $LiFePO_4$ during discharge is obtained. At high C-rates, lithiation could be incomplete and subsequently less specific capacity is available for the next charging step. Again, at low C-rates, a dependency on the carbon content and, at high C-rates, a dependency on the aspect ratio or elongation of the rod-shaped $LiFePO_4$ nanoparticles are observed.

Table 2 summarizes the results of all electrochemical tests. The main difference of all five studied materials is their obtained charge capacity at 10 C. The observed dependence of the fast-charging performance on the aspect ratio c/a or the elongation along c of the rod-shaped $LiFePO_4$/C core/shell particles can be explained by the preferred orientation of the phase boundary between $LiFePO_4$ and $FePO_4$ and the preferred diffusion direction of the phase boundary itself. The phase boundary between $LiFePO_4$ and $FePO_4$ is usually parallel to the bc surface.[37−39] In dependence of the particle size and morphology of the $LiFePO_4$ particles, other orientations were observed experimentally and theoretically.[37,38,4043] In the five presented rod-shaped $LiFePO_4$/C

Table 2. Summary of all Results from Electrochemical Tests with $LiPO_4$/C Core/Shell Nanoparticle Materials with Different Aspect Ratios c/a

#	1	2	3	4	5	trend
c/a	6.9	3.6	3.2	2.4	2.5	↓
1C[a]/mA h·g−1	77.4	82.2	58.6	81.9	84.9	↑
10C[b]/mA h·g−1	0.0	0.0	29.7	50.9	50.3	↑
10C[c]/mA h·g−1	1.5	7.4	50.3	73.0	71.1	↑

[a]Specific charge capacity after 500 cycles at 1 C. [b]Specific charge capacity after 108 cycles at 0.05−10 C and charge rate = discharge rate. [c]Specific charge capacity after 78 cycles at 0.05−10 C, different charge rates, and discharge rate = 0.5 C.

nanoparticle materials, the formation of the phase boundary parallel to the ab surface should be preferred because of the anisotropic particle shape. The correlation of the orientation of the phase boundary and particle morphology was recently studied by Abdellahi et al.[38] The orientation of the phase boundary was influenced by the chemical interfacial energy and the coherency strain energy with respect to particle morphology. Due to the anisotropy of the used $LiFePO_4$-c-needles, the area of a phase boundary parallel to ab is smaller than that parallel to ac or bc because of the relationship $b < a < c$. The diffusion of the phase boundary along the c axis explains why particles with a low aspect ratio and short elongation along the c axis provide the highest specific capacity at high C-rates. The enhanced fast-charging capability results from the reduction of the diffusion path for the phase boundary, so that a complete phase transformation in the shorter rod-shaped particles is obtained faster than in larger particles.

It should be mentioned that an electrode consists not only of one particle but many particles which are connected by a carbon network. Lithium diffusion in carbon is faster than in $LiFePO_4$, so logically, lithium ions can diffuse faster through the electrode in a network of many small $LiFePO_4$ particles and carbon than in an electrode that consists of fewer larger particles.

In summary, it can be concluded from the results that the fast-charging capacity of $LiFePO_4$ particles depends on the diffusion path of the lithium ions and the phase boundary. For rod-shaped particles or c-needles, therefore, a reduction of the dimension along the b and c axis could increase the electrochemical performance.

It should be noted that even for our best materials, absolute values of the specific capacity are lower than those for novel and commercial state-of-the-art materials. This is mainly due to our manual production of the electrode films, cell assembly, the used selection of the various test cell components (binder, separator, electrolyte, carbon black, etc.), and also the used measurement protocols to determine the electrochemical performance. The absolute capacity values could be enhanced by an optimized cell assembly in a clean room or by constant temperature control during cycling. Nevertheless, this would not change the observed trends. All materials were synthesized and manufactured under identical conditions so that the results are comparable. The used measurement protocols led to a reduction of the absolute capacity values because we only (dis)charged at constant current (CC) without an additional constant voltage (CV) step. CV steps with a low current rate at the end of the charge or discharge step increase the absolute charge and discharge capacity but increase the charging time;

https://doi.org/10.1021/acsomega.1c03432
ACS Omega XXXX, XXX, XXX−XXX

therefore, the assignment of a certain C-rate would be misleading.

Excursus. During the comprehensive characterization of the rodlike $LiFePO_4$/C core/shell particles, an average of 2 wt % sulfur was detected by CHNS and TG analysis in all materials. Even though iron(II) sulfate is commonly used as the iron(II) source in hydrothermal and solvothermal synthesis of $LiFePO_4$ nanoparticles, only one publication discussed a sulfur contamination and its possible origin.[28] Huang et al. postulated that sulfate ions had replaced phosphate ions in the olivine crystal structure but did not present clear evidence. Furthermore, some authors described sulfur doping on the oxygen site of the phosphate ion. They used Li_2S or organic sulfur sources.[44−46] The adsorption of sulfur through Fe−S bonds on the $LiFePO_4$ crystal surface was also discussed as a method to optimize the electrochemical properties of $LiFePO_4$ materials.[47,48]

We could detect sulfur oxides (SO and SO_2) during thermal treatment up to 1000 °C (Figure S2). The mass loss correlates with the release of SO_3, a typical combustion gas of inorganic sulfates. In addition, an inhomogeneous sulfur distribution within one particle and sulfur-rich domains with a size of up to 10 nm were detected on high-resolution TEM images in combination with EDS analysis (Figure 8). The sulfur-rich

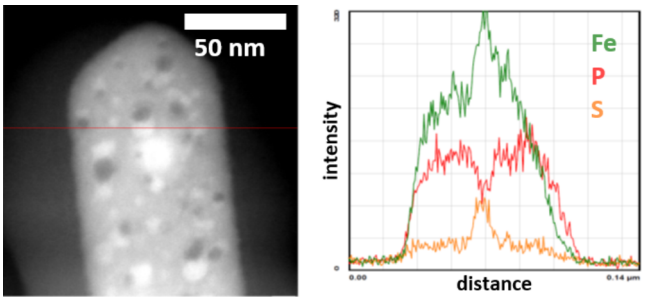

Figure 8. STEM image of a $LiFePO_4$/C core/shell nanoparticle (left) with the corresponding EDS line scan (right).

domains were formed during the solvothermal synthesis and grew during calcination (Figure S3). In a few XRD patterns of $LiFePO_4$/C core/shell particles with low carbon content, additional peaks were detected and assigned to FeS (Figure S4). Based on our results, it can be concluded that the sulfur contamination is sulfate- or sulfide-like. The integration of sulfate ions into the olivine structure is most likely. Furthermore, the reduction of sulfates to sulfides during calcination could explain the partial formation of FeS, especially for $LiFePO_4$/C core/shell particles with low carbon content. Because of a very similar sulfur content in all materials, no influence of the sulfur content on the electrochemical performance could be observed. Therefore, the role of sulfur should be studied in more detail. To avoid sulfur in $LiFePO_4$ materials, alternatives for iron(II) sulfate could be used, for example, iron(II) salts with a thermally unstable anion that decomposes residue-free to volatile gases during high-temperature calcination.

CONCLUSIONS

In conclusion, we established a new reproducible, multistep synthesis strategy for the production of $LiFePO_4$/C core/shell nanoparticles via a solvothermal synthesis and *in situ* polymer coating. A strong influence of the aspect ratio c/a on the fast-charging ability of rodlike $LiFePO_4$ particles with a constant dimension along b was identified. $LiFePO_4$/C nanoparticles with the smallest aspect ratio c/a showed the best electrochemical performance regarding the specific capacity at high C-rates and the cycling stability. We could show that the fast-charging capability of $LiFePO_4$/C core/shell nanoparticles can not only be enhanced by reduction of particle dimension along the b axis but also by reduction of the aspect ratio c/a or reduction of the dimension along the c axis. To our knowledge, this observation has not been reported before. The findings of this work suggest that plate-like ($c \times a$) particles could show a better electrochemical performance and higher fast-charging capability than rodlike particles with a similar elongation along the b axis.

Furthermore, an unavoidable sulfur contamination was identified in all materials, which is not most probably caused by sulfate ions that have been integrated into the olivine structure. Alternatives for iron(II) sulfate could be iron(II) salts with a thermally unstable anion that decomposes residue-free to volatile gases during high-temperature calcination.

EXPERIMENTAL SECTION

Materials. $FeSO_4 \cdot 7H_2O$ (Merck), $LiOH \cdot H_2O$ (AppliChem), ortho-H_3PO_4 (85%, Gruessing), ethylene glycol (99.7%, VWR), ethanol (96, 1% MEK, BCD Chemie), CTAB (98%, Alfa Aesar), ammonia solution (25%, VWR), resorcinol (98%, Gruessing), formaldehyde (37%, Th. Geyer), carbon black (Super P Li, Timcal), polyvinylidene fluoride (PVDF, average M_w ~534,000, Aldrich), and *N*-methyl-2-pyrrolidone (NMP, Merck) were used as received without further purifications. Lithium foil (99.9%, 0.75 mm thick, Alfa Aesar) and Selectilyte LP30 (1 M $LiPF_6$ in EC/DMC (1:1, w/w), BASF) were used and stored in an argon glovebox.

Synthesis. $LiFePO_4$ nanoparticles were obtained via an optimized solvothermal synthesis.[25] $LiOH \cdot H_2O$ and $FeSO_4 \cdot 7H_2O$ were dissolved separately in ethylene glycol. Under vigorous stirring, ortho-H_3PO_4 and subsequently the LiOH solution were added to the iron(II) solution. The resulting viscous solution was transferred immediately to a Teflon-lined stainless-steel autoclave and placed in a preheated oven for the solvothermal treatment (10 h, 180 °C). The stoichiometric ratio of the precursors was 2.5:1:1 to 3:1:1 (Li/Fe/P) with a fixed iron(II) concentration of 0.1 M. The solvothermal precipitates were collected by membrane filtration, washed several times with demineralized water and ethanol, and dried at 60 °C.

The approach of first coating an *in situ*-formed polymer on a nanoparticle surface and second transforming it into a carbon shell via calcination[30−33] was applied for the synthesis of $LiFePO_4$/C core/shell particles. $LiFePO_4$ nanoparticles and a sufficient amount of CTAB were added to a water−ethanol mixture (2:1, v/v). This dispersion was sonicated until no precipitate was left. Under constant stirring, resorcinol and ammonia solution were added. Subsequently, the dispersion was heated to 35 °C and kept at that temperature while the formaldehyde solution was added. The stoichiometric ratio of the polymer precursors was always 1:2.1 (R/F). The polymerization was carried out in a 2 L batch reactor for 6 h at 35 °C. Afterward, $LiFePO_4$/RF core/shell nanoparticles were collected by membrane filtration or centrifugation, washed several times with demineralized water and ethanol, and dried at 60 °C. Finally, the $LiFePO_4$/RF core/shell nanoparticles were transformed to $LiFePO_4$/C core/shell

https://doi.org/10.1021/acsomega.1c03432
ACS Omega XXXX, XXX, XXX−XXX

nanoparticles by calcination in flowing argon (3 h 400 °C, 10 h 700 °C at a heating rate of 2 K·min^{-1}). All initial weights and volumes for the synthesis of each $LiFePO_4$/C material are listed in Supporting Information (Tables S1 and S2).

Characterization. X-ray diffraction was performed with a PANalytical MPD X'Pert Pro with Cu Kα1 radiation. The morphology of the materials was investigated with a scanning electron microscope (LEO Gemini 1525 microscope) and a transmission electron microscope (JEOL JEM 2200 FS). The determination of the zone axis was carried out with the software CrysTBox diffractGUI.[36] The carbon content and chemical composition were estimated by thermogravimetric differential thermal analysis coupled with mass spectrometry (TG-DTA-MS, Netzsch STA 449 F3 Jupiter with a QMS 403 Aëolos) and additionally determined by CHNS analysis (EuroVector EuroEA Elemental Analyzer).

Electrodes were prepared by the following procedure: $LiFePO_4$/C particles and Super P Li were premixed in a mortar, and subsequently, PVDF and NMP were added (80:10:10). After rigorous stirring for 24 h in a closed vial, a homogeneous slurry was obtained, which was coated on aluminum foil. The electrode sheet was dried in a vacuum oven at 100 °C for 24 h, and afterward, electrode circles with a diameter of 18 mm were punched out. The electrode weight ranged from 19 to 23 mg (incl. alumina foil) which corresponds to a mass loading ($LiFePO_4$/C only) of 1.6−2.6 mg·cm^{-2}. For electrochemical testing, PAT-Cells (EL-Cell) were used with a Whatman GF/A separator, lithium foil as the anode, and LP30 as the electrolyte. The cell assembly was performed in an argon glovebox. The assembled cells were cycled with an Arbin BT-2000 potentiostat in a PAT-Tray (EL-CELL) (2.5−4 V) at room temperature.

Cells were charged three times at 0.1 C CC + CV and subsequently 500 times at 1 C CC (stability test). For evaluation of the fast-charging behavior, cells were charged at different C-rates (0.05−10 C CC). The cells were discharged with the same C-rate as charged (fast-charging test I) or at 0.5 C CC (fast-charging test II). C-rates and specific capacities are defined in relation to the total mass of the active material ($LiFePO_4$/C).

■ ASSOCIATED CONTENT

Supporting Information

The Supporting Information is available free of charge at https://pubs.acs.org/doi/10.1021/acsomega.1c03432.

Initial weights and volumes for the syntheses; additional characterization: nitrogen isotherms, TG-DTA-MS analysis, TEM and STEM images, and X-ray patterns of $LiFePO_4$/C core/shell nanoparticles (PDF)

■ AUTHOR INFORMATION

Corresponding Author

Michael Fröba − *Institut für Anorganische und Angewandte Chemie, Universität Hamburg, 20146 Hamburg, Germany;* orcid.org/0000-0001-6927-0509; Email: michael.froeba@chemie.uni-hamburg.de

Author

Julia Seher − *Institut für Anorganische und Angewandte Chemie, Universität Hamburg, 20146 Hamburg, Germany; Bundesanstalt für Materialforschung und -prüfung, 12205 Berlin, Germany*

Complete contact information is available at: https://pubs.acs.org/10.1021/acsomega.1c03432

Author Contributions

The manuscript was written through contributions of all authors. All authors have given approval to the final version of the manuscript.

Funding

This study was financed by the BMVI (Federal Ministry of Transport and Digital Infrastructure), as part of the project SINGER (Sino-German Electromobility Research) in Germany (Förderkennzeichen: 03EM0204C).

Notes

The authors declare no competing financial interest.

■ ACKNOWLEDGMENTS

We thank Andreas Kornowski for providing TEM images and the electron diffraction pattern of our materials.

■ REFERENCES

(1) Park, O. K.; Cho, Y.; Lee, S.; Yoo, H.-C.; Song, H.-K.; Cho, J. Who Will Drive Electric Vehicles, Olivine or Spinel? *Energy Environ. Sci.* **2011**, *4*, 1621−1633.

(2) Padhi, A. K.; Nanjundaswamy, K. S.; Goodenough, J. B. Phospho-Olivines as Positive-Electrode Materials for Rechargeable Lithium Batteries. *J. Electrochem. Soc.* **1997**, *144*, 1188−1194.

(3) Jugović, D.; Uskoković, D. A Review of Recent Developments in the Synthesis Procedures of Lithium Iron Phosphate Powders. *J. Power Sources* **2009**, *190*, 538−544.

(4) Satyavani, T. V. S. L.; Srinivas Kumar, A.; Subba Rao, P. S. V. Methods of Synthesis and Performance Improvement of Lithium Iron Phosphate for High Rate Li-Ion Batteries: A Review. *Eng. Sci. Technol. an Int. J.* **2016**, *19*, 178−188.

(5) Yi, T.-F.; Li, X.-Y.; Liu, H.; Shu, J.; Zhu, Y.-R.; Zhu, R.-S. Recent Developments in the Doping and Surface Modification of LiFePO 4 as Cathode Material for Power Lithium Ion Battery. *Ionics* **2012**, *18*, 529−539.

(6) Wang, J.; Sun, X. Understanding and Recent Development of Carbon Coating on $LiFePO_4$ Cathode Materials for Lithium-Ion Batteries. *Energy Environ. Sci.* **2012**, *5*, 5163−5185.

(7) Li, H.; Zhou, H. Enhancing the Performances of Li-Ion Batteries by Carbon-Coating: Present and Future. *Chem. Commun.* **2012**, *48*, 1201−1217.

(8) Yang, Z.; Dai, Y.; Wang, S.; Yu, J. How to Make Lithium Iron Phosphate Better: A Review Exploring Classical Modification Approaches in-Depth and Proposing Future Optimization Methods. *J. Mater. Chem. A* **2016**, *4*, 18210−18222.

(9) Xu, Z.; Gao, L.; Liu, Y.; Li, L. Review—Recent Developments in the Doped $LiFePO_4$ Cathode Materials for Power Lithium Ion Batteries. *J. Electrochem. Soc.* **2016**, *163*, A2600−A2610.

(10) Li, Z.; Yang, J.; Guang, T.; Fan, B.; Zhu, K.; Wang, X. Controlled Hydrothermal/Solvothermal Synthesis of High-Performance $LiFePO_4$ for Li-Ion Batteries. *Small Methods* **2021**, *5*, 2100193.

(11) Zhou, X.; Wang, F.; Zhu, Y.; Liu, Z. Graphene Modified $LiFePO_4$ Cathode Materials for High Power Lithium Ion Batteries. *J. Mater. Chem.* **2011**, *21*, 3353−3358.

(12) Lung-Hao Hu, B.; Wu, F.-Y.; Lin, C.-T.; Khlobystov, A. N.; Li, L.-J. Graphene-Modified $LiFePO_4$ Cathode for Lithium Ion Battery beyond Theoretical Capacity. *Nat. Commun.* **2013**, *4*, 1687.

(13) Wu, H.; Liu, Q.; Guo, S. Composites of Graphene and $LiFePO_4$ as Cathode Materials for Lithium-Ion Battery: A Mini-Review. *Nano−Micro Lett.* **2014**, *6*, 316−326.

(14) Mo, R.; Tung, S. O.; Lei, Z.; Zhao, G.; Sun, K.; Kotov, N. A. Pushing the Limits: 3D Layer-by-Layer-Assembled Composites for Cathodes with 160 C Discharge Rates. *ACS Nano* **2015**, *9*, 5009−5017.

(15) Wang, X.; Feng, Z.; Huang, J.; Deng, W.; Li, X.; Zhang, H.; Wen, Z. Graphene-Decorated Carbon-Coated $LiFePO_4$ Nanospheres as a High-Performance Cathode Material for Lithium-Ion Batteries. *Carbon* **2018**, *127*, 149−157.
(16) Eftekhari, A. $LiFePO_4$/C Nanocomposites for Lithium-Ion Batteries. *J. Power Sources* **2017**, *343*, 395−411.
(17) Orikasa, Y.; Maeda, T.; Koyama, Y.; Minato, T.; Murayama, H.; Fukuda, K.; Tanida, H.; Arai, H.; Matsubara, E.; Uchimoto, Y.; et al. Phase Transition Analysis between $LiFePO_4$ and $FePO_4$ by In-Situ Time-Resolved X-Ray Absorption and X-Ray Diffraction. *J. Electrochem. Soc.* **2013**, *160*, A3061−A3065.
(18) Liu, H.; Strobridge, F. C.; Borkiewicz, O. J.; Wiaderek, K. M.; Chapman, K. W.; Chupas, P. J.; Grey, C. P. Capturing Metastable Structures during High-Rate Cycling of $LiFePO_4$ Nanoparticle Electrodes. *Science* **2014**, *344*, 1252817.
(19) Zhang, X.; Van Hulzen, M.; Singh, D. P.; Brownrigg, A.; Wright, J. P.; Van Dijk, N. H.; Wagemaker, M. Rate-Induced Solubility and Suppression of the First-Order Phase Transition in Olivine $LiFePO_4$. *Nano Lett.* **2014**, *14*, 2279−2285.
(20) Muraliganth, T.; Murugan, A. V.; Manthiram, A. Nanoscale Networking of $LiFePO_4$ Nanorods Synthesized by a Microwave-Solvothermal Route with Carbon Nanotubes for Lithium Ion Batteries. *J. Mater. Chem.* **2008**, *18*, 5661−5667.
(21) Huang, X.; Yao, Y.; Liang, F.; Dai, Y. Concentration-Controlled Morphology of $LiFePO_4$ Crystals with an Exposed (100) Facet and Their Enhanced Performance for Use in Lithium-Ion Batteries. *J. Alloys Compd.* **2018**, *743*, 763−772.
(22) Saravanan, K.; Balaya, P.; Reddy, M. V.; Chowdari, B. V. R.; Vittal, J. J. Morphology Controlled Synthesis of $LiFePO_4$/C Nanoplates for Li-Ion Batteries. *Energy Environ. Sci.* **2010**, *3*, 457−464.
(23) Yang, S.; Zhou, X.; Zhang, J.; Liu, Z. Morphology-Controlled Solvothermal Synthesis of $LiFePO_4$ as a Cathode Material for Lithium-Ion Batteries. *J. Mater. Chem.* **2010**, *20*, 8086−8091.
(24) Wang, L.; He, X.; Sun, W.; Wang, J.; Li, Y.; Fan, S. Crystal Orientation Tuning of $LiFePO_4$ Nanoplates for High Rate Lithium Battery Cathode Materials. *Nano Lett.* **2012**, *12*, 5632−5636.
(25) Nan, C.; Lu, J.; Li, L.; Li, L.; Peng, Q.; Li, Y. Size and Shape Control of $LiFePO_4$ Nanocrystals for Better Lithium Ion Battery Cathode Materials. *Nano Res.* **2013**, *6*, 469−477.
(26) Ma, Z.; Shao, G.; Fan, Y.; Wang, G.; Song, J.; Liu, T. Tunable Morphology Synthesis of $LiFePO_4$ Nanoparticles as Cathode Materials for Lithium Ion Batteries. *ACS Appl. Mater. Interfaces* **2014**, *6*, 9236−9244.
(27) Mei, R.; Song, X.; Yang, Y.; An, Z.; Zhang, J. Plate-like $LiFePO_4$ Crystallite with Preferential Growth of (010) Lattice Plane for High Performance Li-Ion Batteries. *RSC Adv.* **2014**, *4*, 5746−5752.
(28) Huang, X.; He, X.; Jiang, C.; Tian, G. Morphology Evolution and Impurity Analysis of $LiFePO_4$ Nanoparticles via a Solvothermal Synthesis Process. *RSC Adv.* **2014**, *4*, 56074−56083.
(29) Jiang, Y.; Tian, R.; Liu, H.; Chen, J.; Tan, X.; Zhang, L.; Liu, G.; Wang, H.; Sun, L.; Chu, W. Synthesis and Characterization of Oriented Linked $LiFePO_4$ Nanoparticles with Fast Electron and Ion Transport for High-Power Lithium-Ion Batteries. *Nano Res.* **2015**, *8*, 3803−3814.
(30) Guan, B.; Wang, X.; Xiao, Y.; Liu, Y.; Huo, Q. A Versatile Cooperative Template-Directed Coating Method to Construct Uniform Microporous Carbon Shells for Multifunctional Core-Shell Nanocomposites (Incl. ESI). *Nanoscale* **2013**, *5*, 2469−2475.
(31) Li, N.; Zhang, Q.; Liu, J.; Joo, J.; Lee, A.; Gan, Y.; Yin, Y. Sol−Gel Coating of Inorganic Nanostructures with Resorcinol−Formaldehyde Resin. *Chem. Commun.* **2013**, *49*, 5135−5137.
(32) Zhang, X.-B.; Tong, H.-W.; Liu, S.-M.; Yong, G.-P.; Guan, Y.-F. An Improved Stöber Method towards Uniform and Monodisperse Fe_3O_4@C Nanospheres. *J. Mater. Chem. A* **2013**, *1*, 7488−7493.
(33) Fang, X.; Liu, S.; Zang, J.; Xu, C.; Zheng, M.-S.; Dong, Q.-F.; Sun, D.; Zheng, N. Precisely Controlled Resorcinol-Formaldehyde Resin Coating for Fabricating Core-Shell, Hollow, and Yolk-Shell Carbon Nanostructures. *Nanoscale* **2013**, *5*, 6908−6916.
(34) Qin, X.; Wang, J.; Xie, J.; Li, F.; Wen, L.; Wang, X. Hydrothermally Synthesized $LiFePO_4$ Crystals with Enhanced Electrochemical Properties: Simultaneous Suppression of Crystal Growth along [010] and Antisite Defect Formation. *Phys. Chem. Chem. Phys.* **2012**, *14*, 2669−2677.
(35) Wang, J.; Sun, X. Olivine $LiFePO_4$: The Remaining Challenges for Future Energy Storage. *Energy Environ. Sci.* **2015**, *8*, 1110−1138.
(36) Klinger, M.; Jäger, A. Crystallographic Tool Box (CrysTBox): Automated Tools for Transmission Electron Microscopists and Crystallographers. *J. Appl. Crystallogr.* **2015**, *48*, 2012−2018.
(37) Chen, G.; Song, X.; Richardson, T. J. Electron Microscopy Study of the $LiFePO_4$ to $FePO_4$ Phase Transition. *Electrochem. Solid-State Lett.* **2006**, *9*, A295−A298.
(38) Abdellahi, A.; Akyildiz, O.; Malik, R.; Thornton, K.; Ceder, G. Particle-Size and Morphology Dependence of the Preferred Interface Orientation in $LiFePO_4$ Nano-Particles. *J. Mater. Chem. A* **2014**, *2*, 15437−15447.
(39) Lv, W.; Niu, Y.; Jian, X.; Zhang, K. H. L.; Wang, W.; Zhao, J.; Wang, Z.; Yang, W.; He, W. Space Matters: Li + Conduction versus Strain Effect at $FePO_4$/$LiFePO_4$ Interface. *Appl. Phys. Lett.* **2016**, *108*, 083901.
(40) Laffont, L.; Delacourt, C.; Gibot, P.; Wu, M. Y.; Kooyman, P.; Masquelier, C.; Tarascon, J. M. Study of the $LiFePO_4$/$FePO_4$ Two-Phase System by High-Resolution Electron Energy Loss Spectroscopy. *Chem. Mater.* **2006**, *18*, 5520−5529.
(41) Gabrisch, H.; Wilcox, J.; Doeff, M. M. TEM Study of Fracturing in Spherical and Plate-like $LiFePO_4$ Particles. *Electrochem. Solid-State Lett.* **2008**, *11*, A25−A29.
(42) Ramana, C. V.; Mauger, A.; Gendron, F.; Julien, C. M.; Zaghib, K. Study of the Li-Insertion/Extraction Process in $LiFePO_4$/$FePO_4$. *J. Power Sources* **2009**, *187*, 555−564.
(43) Park, S. B.; Park, C. K.; Hwang, J. T.; Cho, W. I.; Jang, H. Anisotropic Lithium Ion Migration in $LiFePO_4$. *Met. Mater. Int.* **2011**, *17*, 1017−1020.
(44) Lee, S.; Cho, S.; Aravindan, V.; Kim, H.; Lee, Y. Improved Cycle Performance of Sulfur-Doped $LiFePO_4$ Material at High Temperatures. *Bull. Korean Chem. Soc.* **2009**, *30*, 2223−2226.
(45) Yu, T.; Wang, Z.; Fu, Y.; Xioang, Y.; Guan, S. Sulfur Substituted $LiFePO_4$/C with Improved Rate Performance for Lithium Ion Batteries. *Int. J. Electrochem. Sci.* **2016**, *11*, 5999−6008.
(46) Okada, K.; Kimura, I.; Machida, K. High Rate Capability by Sulfur-Doping into $LiFePO_4$ Matrix. *RSC Adv.* **2018**, *8*, 5848−5853.
(47) Park, K.-S.; Xiao, P.; Kim, S.-Y.; Dylla, A.; Choi, Y.-M.; Henkelman, G.; Stevenson, K. J.; Goodenough, J. B. Enhanced Charge-Transfer Kinetics by Anion Surface Modification of $LiFePO_4$. *Chem. Mater.* **2012**, *24*, 3212−3218.
(48) Xu, G.; Zhong, K.; Zhang, J. M.; Huang, Z. First-Principles Investigation of the Electronic and Li-Ion Diffusion Properties of $LiFePO_4$ by Sulfur Surface Modification. *J. Appl. Phys.* **2014**, *116*, 063703.

https://doi.org/10.1021/acsomega.1c03432
ACS Omega XXXX, XXX, XXX−XXX